Simultaneous density and velocity measurements in a supersonic turbulent boundary layer*

He Lin(何 霖), Yi Shi-He(易仕和)†, Tian Li-Feng(田立丰), Chen Zhi(陈 植), and Zhu Yang-Zhu(朱杨柱)

College of Aerospace Science and Engineering, National University of Defense Technology, Changsha 410073, *China*

(Received 27 June 2012; revised manuscript received 23 August 2012)

A novel technique for simultaneous measurements of instantaneous whole-field density and velocity fields of supersonic flows has been developed. The density measurement is performed based on the nano-tracer planar laser scattering (NPLS) technique, while the velocity measurement is carried out using particle image velocimetry (PIV). The present experimental technique has been applied to a flat-plate turbulent boundary layer at Mach 3, and the measurement accuracy of the density and velocity are discussed. Based on this new technique, the Reynolds stress distributions were also obtained, demonstrating that this is an effective means for measuring Reynolds stresses under compressible conditions.

Keywords: simultaneous measurements, density, velocity, Reynolds stress

PACS: 47.40.ki, 47.27.nb, 47.80.Jk **DOI:** 10.1088/1674-1056/22/2/024704

1. Introduction

For a thorough investigation of turbulent flows, conventional methods that measure only one parameter are not enough. Therefore, simultaneous measurements of two or more parameters are required, and they could provide more information about turbulent flows and help to validate and develop turbulence models.

There are several methods for measuring velocity and temperature simultaneously. For example, the combination of coherent anti-Stokes Raman scattering (CARS) and laser Doppler velocimetry (LDV),[1–4] thermocouple and LDV[5–8] are usually used. Broadband time-resolved CARS spectrography can also be used to measure the global molecular vibrational spectra and dephasing times of molecular vibrational modes simultaneously.[9] Recently, to the whole-field velocity and temperature simultaneous measurements, the combination of the laser-induced fluorescence and LDV,[10] scanning liquid-crystal thermometry, and particle image velocimetry (PIV),[11] and the Molecular Tagging Velocimetry/Thermometry (MTV/T)[12] were used. Besides the velocity and temperature, the velocity and concentration field or passive scalar field are usually selected for simultaneous measurements. For this purpose, the simultaneous measurements of the velocity via PIV or particle tracking velocimetry (PTV) and the concentration field via planar laser-induced fluorescence (PLIF) have been performed, as can be found in many previous experimental studies.[13–20]

For compressible flows, the variation of density due to compressibility effects will affect the characteristics of turbulent flows and, therefore, the simultaneous measurements including the density fields are needed. However, there are few techniques which can measure density and velocity simultaneously. Ramaprabhu *et al.*[21] performed an experimental study for simultaneous measurement of density and velocity in a turbulent Rayleigh–Taylor mixing layer, where the velocity field was measured by PIV and the density was obtained by spatially averaging over an interrogation window of the particle images. The simultaneous PIV/PLIF measurements have also been used to extract the density and velocity fields simultaneously (Horner–Devine,[22] Balakumar *et al.*,[23] Xu and Chen[24]).

To date, simultaneous density and velocity measurements in supersonic flows have scarcely been reported due to the difficulties involved in such measurement under supersonic conditions. On the one hand, PIV and PTV, as the most successful non-invasive velocity measurement techniques, are limited by the flow-following ability of the tracer particles in supersonic flows. On the other hand, although conventional density measurement techniques like schlieren, shadowgraphy or interferometry have been used worldwide for many decades, these methods are not suitable for three-dimensional flow measurements. The PLIF technique can be used for three-dimensional density measurement, but it still suffers limitations of low signal-to-noise ratio (SNR) and complicated calibration procedure in supersonic flows.

In this paper, we present a new experimental method for simultaneous measurements of the instantaneous density and velocity fields, based on a combination of PIV and the nano-tracer planar laser scattering (NPLS) technique. The present method was applied to a Mach 3 flat-plate turbulent boundary layer, and the measurement accuracy of both the density and velocity are discussed. An important advantage of this

*Project supported by the National Basic Research Program of China (Grant No. 2009CB724100) and the National Natural Science Foundation of China (Grant No. 11172326).

†Corresponding author. E-mail: ysh_1819@yahoo.com.cn

© 2013 Chinese Physical Society and IOP Publishing Ltd

method is its ability to make Reynolds stress measurements in supersonic flows while taking into account the effect of density variation and fluctuation due to compressible effects.

2. Experimental setup and methods

2.1. Flow facility

The experiments reported here were performed in a supersonic wind tunnel in the Aerodynamics Laboratory at the National University of Defense Technology. The tunnel operates in a vacuum-indraft mode, and the test section is 250-mm long, 120-mm high, and 100-mm wide. Each wall of the test section has a glass window along the entire test section's length, providing ample optical access from four sides (see Fig. 1). In the present study, the tunnel was operated at Mach 3.0 with a stagnation pressure of 0.1 MPa and stagnation temperature of 300 K. The test boundary layer developed in a nominally zero pressure gradient along the wall of the wind tunnel, with transition occurring naturally upstream in the nozzle section. The parameters of the turbulent boundary layer are summarized in Table 1.[25]

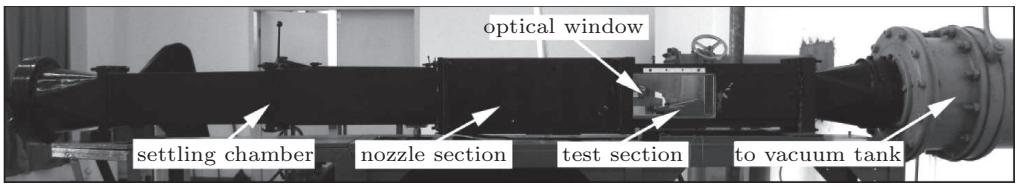


Fig. 1. Picture of the supersonic wind tunnel.

Table 1. Parameters of the turbulent boundary layer.[25]

Parameter	Quantity
M_∞	3
U_∞/m·s^{-1}	620
Re/m^{-1}	7.49×10^6
δ_{99}/mm	10.2
δ^*/mm	3.66
θ/mm	0.68
$H=\delta^*/\theta$	5.38
Re_θ	5100
u_τ/m·s^{-1}	29.9
C_f	1.70×10^{-3}

2.2. Density measurement

The density measurement technique is based on the NPLS technique, which has recently been developed in our laboratory. The NPLS technique is a powerful tool for diagnostics of turbulent flows,[26] and nanoparticles adopted as tracers play a key role in this technique. Due to the good flow-following ability of the nanoparticles, which has been validated in experiments, the local concentration of the nanoparticles is proportional to the local gas density, if the concentration distribution of particles on the inlet of flow field is uniform. Because the local gray value of each NPLS image is determined by the local intensity of scattered light, which is directly proportional to the local concentration of the nanoparticles, the local gas density is a function of the local gray value of each NPLS image (see Fig. 2). After quantifying the relationship between the gas density and the gray value using certain methods, such as the oblique shock wave calibration method, the instantaneous density fields can be calculated from the NPLS images. (For more details see Ref. [27].) This density measurement technique has also been used by Zhao *et al.*[28,29] to investigate a supersonic mixing layer.

$$\boxed{\text{Gray value of NPLS image } (I)} \propto \boxed{\text{intensity of Rayleigh signal}} \propto \boxed{\text{concentration of nanoparticles } (N)} \propto \boxed{\text{gas density } (\rho)} \Rightarrow \rho = f(I)$$

Fig. 2. Principle of the density measurement based on NPLS technique.

2.3. Velocity measurement

Velocity measurements in supersonic flows constitute a technical challenge due to the presence of strong velocity fluctuations. Whether the tracer particles follow the flow faithfully directly determines the accuracy of the PIV measurements. With the aid of the good flow-following ability of the nanoparticles, a PIV technique should provide a reliable method for velocity measurement in supersonic flows.

2.4. Combined NPLS and PIV system

Combining NPLS and PIV techniques presents a possibility of simultaneous density and velocity measurements. In the combined NPLS and PIV system, a double-pulsed Nd:YAG

laser, with 500-mJ pulsed energy and a 6-ns pulse duration at wavelength 532 nm, is applied as the light source for both NPLS and PIV. The laser beam is delivered by an articulated arm and formed into a laser sheet with a minimum thickness of about 0.5 mm using cylindrical and spherical lenses. Unlike the two CCD cameras with a set of optical filters needed in the combined PIV and PLIF system, only one CCD camera is needed in the present system. Here, a 12-bit interline transfer CCD camera, with a resolution of 2048×2048 pixels, is used as the imaging system, which can capture two sequential images in a short time interval (sub-microsecond range). The double-pulsed Nd:YAG laser and CCD camera are connected to a host computer via a synchronizer, which controls the timing of laser illumination and image acquisition. Through a nanoparticle generator driven by compressed gas, the nanoparticles are seeded upstream of the stagnation chamber of the tunnel and are used for both the density and velocity measurements. A schematic depicting the combined NPLS and PIV measurement system is shown in Fig. 3.

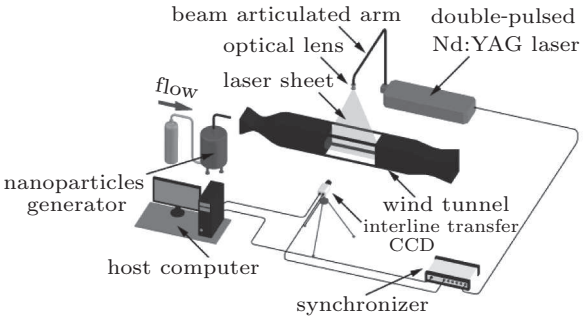


Fig. 3. Schematic plot of the combined NPLS and PIV system.

Using this combined NPLS and PIV system, a series of images can be obtained per run. The two successive images obtained within a very short time interval are used to compute the instantaneous velocity vectors using the cross-correlation algorithm of the PIV method. The same images are also used to calculate the instantaneous density field, after quantifying the relationship between the gas density and the gray value of the images, and the simultaneous density and velocity measurements are realized. This process is shown schematically in Fig. 4. The key factor of the simultaneous density and velocity measurements is using nanoparticles as tracers, and proper selection of the size of nanoparticles is very important. Smaller nanoparticles will provide better flow-following ability, which will be beneficial to both the density and velocity measurements. However, if the diameter of nanoparticles is too small, a single particle cannot be identified in the images due to the limitation of the spatial resolution. This will increase the error of velocity measurement in the cross-correlation method. So, the size of nanoparticles used in the simultaneous measurements should be relatively larger. On the other hand, in order to improve the density measurement accuracy, the concentration of the nanoparticles in each experimental measurement must stay the same as that in the calibration of the relationship between the gas density and the gray value. The particle concentration must also remain constant during each run of the experiment.

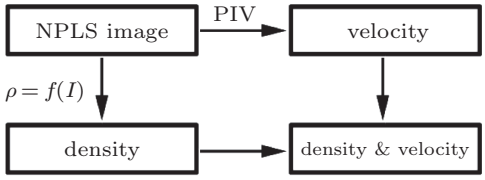


Fig. 4. Schematic plot of the simultaneous density and velocity measurements.

In the present experimental study, this simultaneous measurement technique was applied to a flat-plate turbulent boundary layer at Mach 3. Titanium dioxide (TiO2) particles with a nominal diameter of 50 nm and a bulk density of approximately 200 kg/m^3 were adopted as the tracer particles in the present experiments. A Cartesian coordinate system was adopted with x, y, and z in the streamwise, wall-normal, and spanwise direction, respectively. Measurements were made in the xy-plane along the spanwise centerline of the test section, with a streamwise, wall-normal field of view of $1.6\delta \times 1.5\delta$. Before the simultaneous measurements, a careful calibration of the relationship of the gray values to the gas density is required for density measurements. Here, the calibration was also performed using the oblique shock wave calibration method. For velocity measurements, the time delay between the two laser pulses was set to 0.3 μs, producing a maximum particle displacement of approximately 16 pixels, based on the freestream speed and the spatial resolution (about 11.4 μm/pixel) in the present measurements. Each image pair was interrogated using a 32×16 pixels window with an overlap factor of 50%, yielding a spatial resolution of 16×8 pixels (=0.36 mm×0.18 mm) for velocity measurements. Because the spatial resolution of the density field, determined by the camera resolution, is larger than the resolution of the velocity field, local spatial average of the density field within the same interrogation windows of PIV calculation was performed to provide the same resolution as the velocity field. An ensemble of 400 simultaneous data measurements in the xy-plane was collected to study the statistical properties of the turbulent boundary layer.

3. Results and discussion

3.1. Simultaneous measurement results

A sample of the simultaneous density and velocity measurement results is presented in Fig. 5, and the flow is from

left to right. Figure 5(a) shows an instantaneous NPLS image after the contrast has been enhanced for display purposes. The instantaneous streamwise velocity field, calculated from Fig. 5(a) and the other successive NPLS image (not present here), is shown in Fig. 5(b). The instantaneous density field obtained from Fig. 5(a) is shown in Fig. 5(c). Based on the simultaneous density and velocity data, the instantaneous mass-flux (ρu) is calculated and shown in Fig. 5(d). It is interesting to note that the instantaneous contour plot of mass-flux displays a similar pattern of the instantaneous contour plot of density, which would indicate a strong correlation between the two parameters. On the contrary, there is no similarity between the velocity field and the mass-flux field. The correlations among density, velocity, and mass-flux would provide more useful information for improving our understanding of the mechanics of turbulent flows. However, these remain unclear and should be the focus of further study.

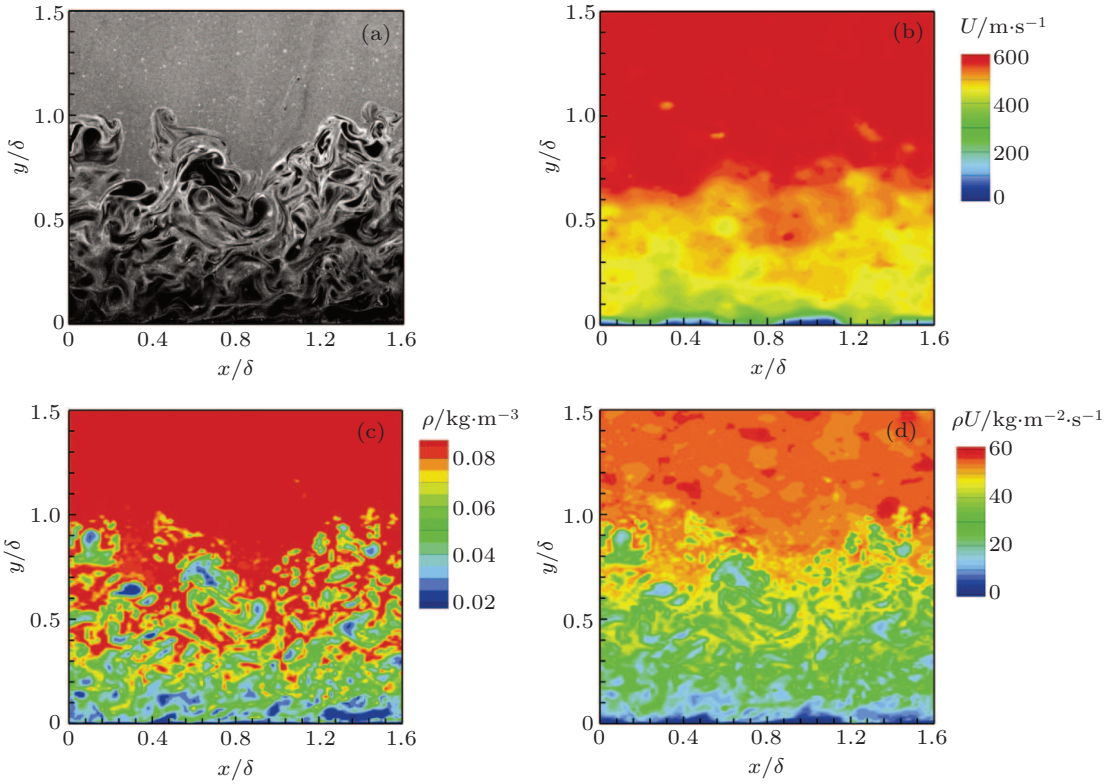


Fig. 5. (color online) Sample of the simultaneous density and velocity measurement results. (a) Instantaneous NPLS image (contrast-enhanced), (b) instantaneous contour plot of streamwise velocity, (c) instantaneous contour plot of density, and (d) instantaneous contour plot of mass-flux calculated from (b) and (c). Flow is from left to right.

3.2. Discussion of the accuracy

As a new technique, the most interesting point is the accuracy of the simultaneous density and velocity measurements. For the purpose of validating the measurement accuracy, we compare the present results with previous data. However, to the best of the authors' knowledge, no other density and velocity data exist for a supersonic turbulent boundary layer at the same Mach and Reynolds number of the present experiments. Therefore, previous data at a similar Mach number are chosen here for comparison. The comparison of the mean and RMS velocity profiles are shown in Figs. 6(a) and 6(b), respectively. The mean streamwise velocity u^+, transformed using the method of van Driest,[30] is plotted versus y^+ and compared with previous DNS data.[31–33] The superscript ($^+$) indicates normalization using u_τ for velocity and ν_w/u_τ for length, where u_τ is the friction velocity and ν_w is the kinematic viscosity at the wall. The present mean velocity profile is in excellent agreement with the DNS data, except for some discrepancies in the outermost region of the boundary layer, where the freestream conditions are different from each other. However, due to the limitation of the PIV spatial resolution, the velocity data in the very near wall region ($y^+ < 15$ or $y/\delta < 0.03$) are presently lacking, and cannot be compared with the DNS data here. As shown in Fig. 6(b), the RMS of streamwise velocity fluctuations $\langle u' \rangle$ in the present experiments is relatively larger than the PIV data reported by Humble *et al.*,[34] where the Mach number was 2.1. The disparity between the respective results may be attributed to the difference in freestream Mach numbers. Instead, qualitatively good agreement of the RMS of transverse velocity fluctuation $\langle v' \rangle$ is observed.

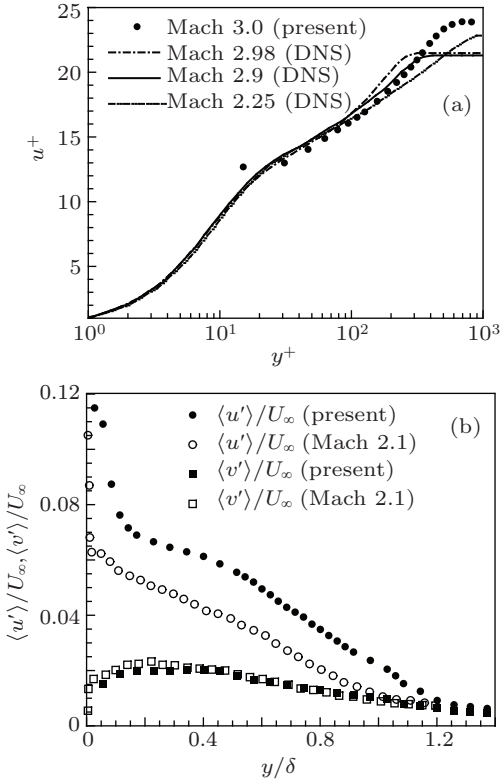


Fig. 6. Comparison of the mean and RMS velocity profiles: (a) Van Driest transformed mean velocity profile compared with numerical simulation results,[31–33] and (b) RMS velocity profile compared with the PIV data by Humble *et al.*[34]

Figure 7(a) shows a comparison of the mean density profile between the present result and the experimental data by Spina and Smits.[35] The previous experimental data was derived from a point probe survey using a hot wire, and the density profile was estimated from the mass-flux data based on the strong Reynolds analogy (SRA). The mean density profiles also show good agreement with each other, despite a slight discrepancy observed for $y/\delta < 0.5$. The RMS of density fluctuations is also compared with the results obtained by Spina and Smits[35] and shown in Fig. 7(b). Note that the vertical axis is logarithmic, so the discrepancies between the present result and the previous data are relatively large as seen in Fig. 7(b). However, these data exhibit similar trends along the y direction. Since the SRA[36] shows that relative density fluctuations are proportional to the square of the Mach number, a relatively large density fluctuation in the present experiments is acceptable. Considering the good accuracy of the velocity measurement in the present experiments, the present density result is compared with the density inferred from PIV velocity measurement, where the mean temperature profile is calculated from the mean streamwise velocity profile using the Crocco–Busemann relationship,[37] and then the density (here called ρ_{CB}) is obtained from the mean temperature profile based on the zero-pressure-gradient hypothesis. In this comparison, the influence of the differences in Mach and Reynolds number is not taken into account. As shown in Fig. 8, the present mean density profile is also in very good agreement with the mean density profile calculated from the present PIV data, indicating good accuracy of the density measurements. Nevertheless, the comparisons mentioned above are still not enough, and more numerical and experimental datasets are needed to further validate the accuracy of these simultaneous density and velocity measurements.

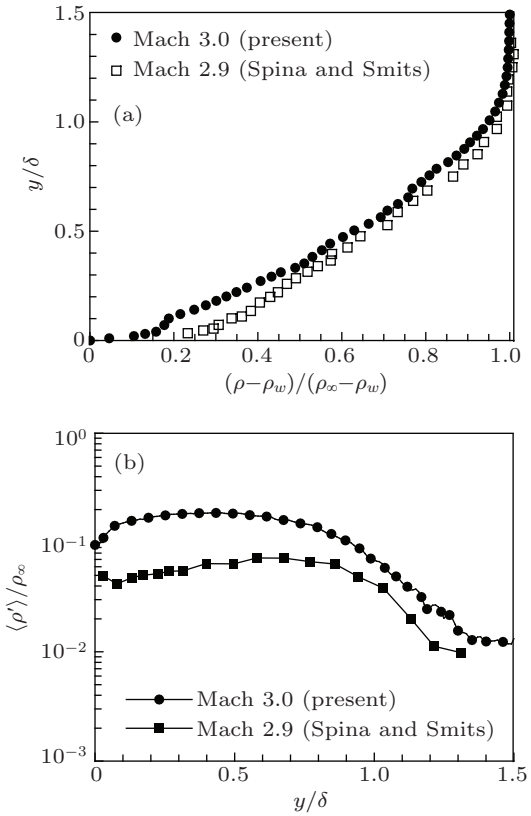


Fig. 7. Comparison of (a) the mean and (b) the RMS density profiles between the present results and previous experimental data.[35]

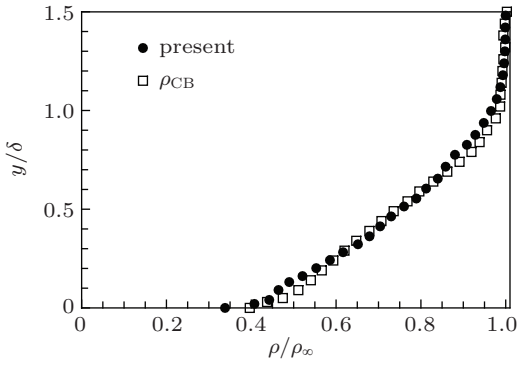


Fig. 8. Mean density profile of the present results compared with the data inferred from PIV velocity measurements.

3.3. Reynolds stress measurements

The measurement of Reynolds stresses is easy in incompressible flows, where only the velocity measurement is required. However, the measurements are much more difficult in compressible flows, where the compressibility effect will affect the behavior of Reynolds stresses and must

be taken into account. For low Mach number flows ($Ma < 5$), the Reynolds stresses are conventionally expressed as $\bar{\rho}\overline{u_i'u_j'}$, when the density fluctuations are ignored according to Morkovin's hypothesis.[36] Therefore, only the mean local density is needed, and it can be calculated from the velocity data using the method described above. But for hypersonic flows, the effect of density fluctuations is strong and can no longer be neglected. Not only the mean density, but also the density fluctuations are needed for the measurement of Reynolds stresses. Based on the simultaneous density and velocity measurements technique described in this paper, the distributions of Reynolds stresses can be obtained directly, taking into account the compressibility effects.

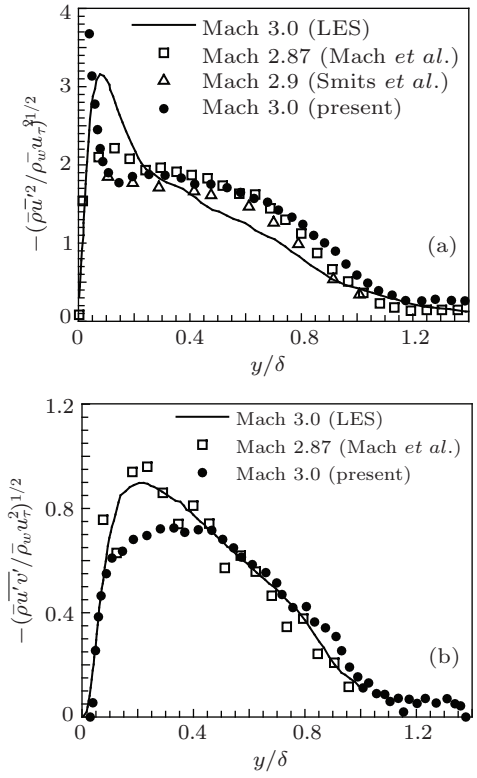


Fig. 9. (color online) (a) Normalized Reynolds normal stress and (b) normalized Reynolds shear stress compared with previous data.[38–40]

The Reynolds normal stress $\left(\bar{\rho}\overline{u'u'}\right)$ and Reynolds shear stress $\left(\bar{\rho}\overline{u'v'}\right)$, compared with previous data, are shown in Figs. 9(a) and 9(b) respectively. The results are normalized using the wall shear stress $\tau_w = \rho_w u_\tau^2$, where u_τ is the friction velocity and ρ_w is the density at the wall. As shown in Fig. 9(a), the present Reynolds normal stress profile shows good agreement with the previous experimental results of Smits *et al.*[38] and Muck *et al.*[39] for $y/\delta \geq 0.2$, despite a relatively lower value of the LES result.[40] In the region $0.1 < y/\delta < 0.2$, the present data still show good agreement with the experimental data of Smits *et al.*, but a relatively higher value of the experimental data of Muck *et al.* is observed. It is interesting to observe that the LES result becomes larger than other data in this region. The rapid increase of the present result in the region $y/\delta < 0.1$ may be problematic, due to the difficulties in obtaining reliable results very close to the wall using the present technique. Figure 9(b) shows a good agreement between the present Reynolds shear stress profile and the previous result for $y/\delta > 0.4$. However, the peak value of the present data is lower than other results. The discrepancies may be attributed to differences in Reynolds number. Although the measurements close to the wall are subject to considerable uncertainty, a good agreement between the present result and the LES data is observed for $y/\delta < 0.1$, where the experimental data of Much *et al.* were not provided.

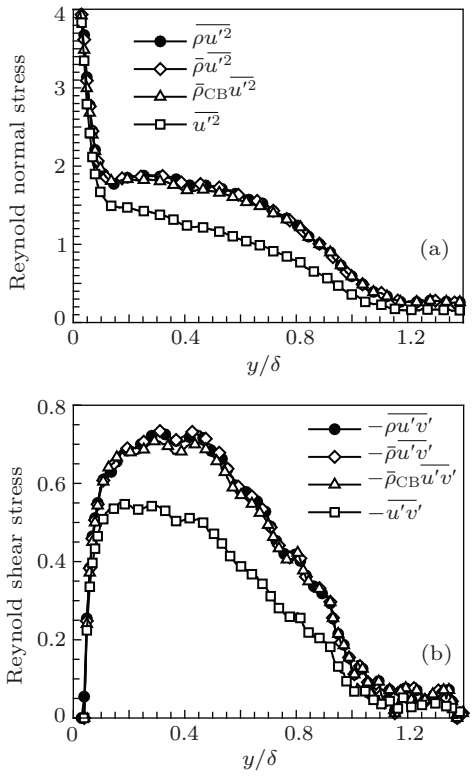


Fig. 10. Comparison of (a) Reynolds normal stress and (b) Reynolds shear stress calculated in different ways.

Based on the simultaneous density and velocity data, the Reynolds stresses can be calculated in different ways with the aim of studying the influence of compressibility effect on the distributions of Reynolds stresses. Here, Reynolds stresses are calculated as: (i) $\overline{\rho u_i'u_j'}$ (considering the effect of density fluctuations); (ii) $\bar{\rho}\overline{u_i'u_j'}$ (without considering the effect of density fluctuations); (iii) $\bar{\rho}_{\rm CB}\overline{u_i'u_j'}$ (using the mean density calculated from the velocity measurements); and (iv) $\overline{u_i'u_j'}$ (without considering the effect of density variations). The Reynolds normal stress and Reynolds shear stress profiles calculated in the above ways are compared in Figs. 10(a) and 10(b), respectively. As shown in Fig. 10(a), the profiles of $\overline{\rho u'u'}$ and $\bar{\rho}\overline{u'u'}$ are nearly the same, indicating that the effect of density fluctuations are very small and can be neglected in the present experiments. The results confirm the validity of Morkovin's

hypothesis in the present Mach 3 turbulent boundary layer. Besides, there is a slight discrepancy between the profiles of $\overline{\rho u'u'}$ and $\bar{\rho}_{\rm CB}\overline{u'u'}$, which is probably due to the difference in the mean density profiles as plotted in Fig. 8. However, large discrepancies between the profiles of $\overline{u'u'}$ and other results are found, revealing that the density variation due to the compressibility effect can have a large effect on the distribution of Reynolds normal stress. A similar trend can also be observed for Reynolds shear stress, as shown in Fig. 10(b). Although there is almost no difference between $\overline{\rho u'u'}$ and $\bar{\rho}\overline{u'u'}$ in the present experiments, the discrepancy should be further highlighted in hypersonic flows. Furthermore, one can appreciate that the distributions of Reynolds stresses in hypersonic flows can be measured more accurately based on the simultaneous density and velocity measurements.

4. Conclusions

The combined NPLS and PIV experimental technique provides a valuable diagnostic tool to simultaneously measure instantaneous whole-field density and velocity in supersonic flows. In this work, this technique has been applied to a flat-plate turbulent boundary layer at Mach 3. The instantaneous density and velocity fields were obtained, and the instantaneous mass-flux field was also calculated based on the simultaneous density and velocity data. The mean and RMS profiles of both density and velocity agree well with the previous measurements. Besides, the mean density profile is also in excellent agreement with the result inferred from PIV velocity measurements. These comparisons show the acceptability of the measurement accuracy of the present experimental technique.

An important advantage of the simultaneous density and velocity measurements is its ability to make Reynolds stress measurements in supersonic flows, where the influence of the compressibility effect can be taken into account. The present Reynolds stress profiles also show good agreement with previous results. The last section provides comparisons of Reynolds stress profiles calculated in four different ways, with the aim of studying the influence of compressibility effect on the distributions of Reynolds stresses. The results show that there is almost no difference between $\overline{\rho u'u'}$ and $\bar{\rho}\overline{u'u'}$ in the present Mach 3 turbulent boundary layer, confirming the validity of Morkovin's hypothesis. A slight discrepancy between the profiles of $\overline{\rho u'u'}$ and $\bar{\rho}_{\rm CB}\overline{u'u'}$ is found, probably due to the difference in the mean density profiles. But relatively large discrepancies exist between the profiles of $\overline{u'u'}$ and other results, which indicates that the density variation due to the compressibility effect can have a large effect on the behavior of Reynolds stresses. Nevertheless, the great advantage of this technique in Reynolds stress measurements will be seen when applied in hypersonic flows.

References

[1] Fujii S, Gomi M and Equchi K 1983 *J. Fluids Eng.* **105** 128
[2] Fujii S, Gomi M, Equchi K, Yamayuchi S and Jin L 1984 *Combust. Sci. Technol.* **36** 211
[3] Goss L P, Trump D D and Roquemore W M 1984 *AIAA J.* **84** 1458
[4] Goss L P, Trump D D and Roquemore W M 1988 *Exp. Fluids* **6** 189
[5] Bram R D, Seller E T, LaRue J C and Samuelsen G S 1983 *AIAA Paper* 83-0334
[6] Heitor M V, Taylor A M K P and Whitelaw J H 1985 *Exp. Fluids* **3** 323
[7] Tagawa M, Nagaya S and Ohta Y 2001 *Exp. Fluids* **30** 143
[8] Li F C, Wang D Z, Kawaguchi Y and Hishida K 2004 *Exp. Fluids* **36** 131
[9] Yin J, Yu L Y, Liu X, Wan H, Lin Z Y and Niu H B 2011 *Chin. Phys.* B **20** 014206
[10] Lemoine F, Antoine Y, Wolff M and Lebouche M 1999 *Exp. Fluids* **26** 315
[11] Fujisawa N, Funatani S and Katoh N 2005 *Exp. Fluids* **38** 291
[12] Ke J and Bohl D 2011 *Exp. Fluids* **50** 465
[13] Webster D R, Roberts P J and Ráad L 2001 *Exp. Fluids* **30** 65
[14] Cowen E A, Chang K A and Liao Q 2001 *Exp. Fluids* **31** 63
[15] Borg A, Bolinder J and Fuchs L 2001 *Exp. Fluids* **31** 140
[16] Feng H, Olsen M G, Hill J C and Fox R O 2007 *Exp. Fluids* **42** 847
[17] Konle M, Kiesewetter F and Sattelmayer T 2008 *Exp. Fluids* **44** 529
[18] Zarruk A G and Cowen E A 2008 *Exp. Fluids* **44** 865
[19] Cessou A, Varea E, Criner K, Godard G and Vervisch P 2012 *Exp. Fluids* **52** 905
[20] Sarathi P, Gurka R, Kopp G A and Sullivan P J 2012 *Exp. Fluids* **52** 247
[21] Ramaprabhu P and Andrews M J 2003 *Exp. Fluids* **34** 98
[22] Horner-Devine A R 2006 *Exp. Fluids* **14** 559
[23] Balakumar B J, Orlicz G C, Tomkins C D and Prestridge K P 2008 *Phys. Fluids* **20** 124103
[24] Xu D and Chen J 2012 *Exp. Fluids* **53** 145
[25] He L, Yi S H, Zhao Y X, Tian L F and Chen Z 2011 *Sci. China* G: *Phys. Mech. Astron.* **54** 1702
[26] Zhao Y X, Yi S H, Tian L F, He L and Cheng Z Y 2009 *Sci. China* E: *Tech. Sci.* **52** 3640
[27] Tian L F, Yi S H, Zhao Y X, He L and Cheng Z Y 2009 *Sci. China* G: *Phys. Mech. Astron.* **52** 1357
[28] Zhao Y X, Yi S H, Tian L F, He L and Cheng Z Y 2010 *Sci. China* E: *Tech. Sci.* **53** 584
[29] Zhao Y X, Yi S H, Tian L F, He L and Cheng Z Y 2010 *Chin. Sci. Bull.* **55** 2004
[30] van Driest E R 1956 *Journal of the Aeronautical Sciences* **23** 1007
[31] Gatski T B and Erlebacher G 2002 *NASA Tech. Memo.* 2002-211934
[32] Ringuette M J, Wu M and Martin M P 2008 *J. Fluid Mech.* **594** 59
[33] Wu M and Martin M P 2007 *AIAA Journal* **45** 879
[34] Humble R A, Scarano F and van Oudheusden B W 2006 *AIAA Paper* 2006-3361
[35] Spina E F and Smits A J 1987 *J. Fluid Mech.* **182** 85
[36] Morkovin M V 1962 *Mćanique de la Turbulence*, ed. Favre A CNRS 367
[37] White F M 1974 *Viscous Fluid Flow* (New York: McGraw-Hill)
[38] Smits A J, Spina E F, Alving A E, Smith R W, Fernando E M and Donovan J F 1989 *Phys. Fluids* A **1** 1865
[39] Muck K, Spina E and Smits A 1984 *Report No. MAE*-1642
[40] Urbin G, Knight D and Zheltovodov A A 1999 *AIAA Paper* 99-0427